Journal of Volcanology and Geothermal Research 467 (2025) 108410

Contents lists available at ScienceDirect

Journal of Volcanology and Geothermal Research

journal homepage: www.journals.elsevier.com/journal-of-volcanology-and-geothermal-research

Non-eruptive transients and fluid flow processes driving volcano-tectonic crises at Vulcano, Italy

Matteo Lupi [a,*], Salvatore Alparone [b], Mimmo Palano [b,c], Andrea Ursino [b], Tullio Ricci [d], Anthony Finizola [e,f], Douglas Stumpp [a], Iván Cabrera-Pérez [a], Geneviève Savard [a]

[a] Department of Earth Sciences, University of Geneva, Geneva, Switzerland
[b] Istituto Nazionale di Geofisica e Vulcanologia, Osservatorio Etneo, Sezione di Catania, Italy
[c] Dipartimento di Scienze della Terra e del Mare, Università degli Studi di Palermo, Palermo, Italy
[d] Istituto Nazionale di Geofisica e Vulcanologia, Sezione Roma 1, Italy
[e] Université de La Réunion, Laboratoire GéoSciences Réunion, Saint Denis, France
[f] Université de Paris, Institut de physique du globe de Paris, CNRS, Paris, France

ARTICLE INFO

Keywords:
Volcanic unrest
VLP
Volcano-tectonics
Over-pressure
Hydrothermal system

ABSTRACT

Although not all volcanic unrests lead to eruptions, it is commonly believed that magma rising through the shallow crust drives volcanic awakening. When eruptions do not occur, hydrothermal activity is often claimed to be responsible for inflation and deflation processes. Yet, a causal process explaining long-lasting non-eruptive unrest is still missing. Vulcano, the southernmost island of the Aeolian volcanic archipelago, Italy, entered in unrest in September 2021. The island experienced intense ground deformation, a sustained increase in fumarole temperatures, gas emissions, and shallow seismicity. CO_2 diffuse soil degassing increased at the foothill of La Fossa cone, causing the evacuation of inhabitants. Very Long Period (VLP) seismic events with a daily rate of up to 450 events/day were found in the seismic records for the first time since the deployment of the broadband network in 2005. With the benefit of hindsight, new VLPs were also discovered hidden in the 2018 seismic records. Geodetic data show inflation occurring in 2021, suggesting the pressurization of the shallow portion of the magmatic plumbing system beneath Vulcano. A similar behaviour occurred also in 2018. However, a few aspects of these unrests are not fully compatible with traditional causative models invoking a shallow dike emplacement or with a hydrothermal scenario. In particular, the long-lasting transient character of VLPs during 2021–22 has never been encountered before in hydrothermal-driven unrests.

We propose that deep-seated fluid pressure, possibly promoted by a destabilizing event at depth, either of magmatic or tectonic origin, may have driven the unrests and be responsible for a discrete and transient release of lithostatic fluid pressures from the plumbing system. In particular, NE-striking normal faults highlighted by a high-resolution nodal ambient noise tomography seem to play a key role in modulating the transient character of the 2021 unrest. Once released, overpressure fronts travel across a rheologically complex domain causing VLPs. Once entering the hydrothermal system, fluids (e.g. H_2O and CO_2 dominated mixtures) phase-separate and expand. This pressurizes the shallow plumbing system leading to intense shallow microseismicity. Our model is supported by the long-lasting transient character of the VLP events occurring in swarms and reconciles multiple interdisciplinary observations impacting how we understand the interplay between tectonics, volcanism and natural hazards.

1. Introduction

The Aeolian Islands compose a volcanic archipelago in the Tyrrhenian Sea offshore Sicily, Italy (Fig. 1). Every year, thousands of tourists visit the active craters of Vulcano and Stromboli. Geological (Ruch et al., 2016; Piochi et al., 2009; Tibaldi, 2015), geochemical (Carapezza et al., 2011; Ricci et al., 2015; Di Martino et al., 2022; Inguaggiato et al., 2022), and geophysical (Chiarabba et al., 2004; Alparone et al., 2019; Totaro et al., 2022) studies have shown the high volcanic hazard of Vulcano and Stromboli (Selva et al., 2020). Vulcano island (herein Vulcano) is the southernmost volcano of the Aeolian arc and, with Lipari, is suggested to be part of a North–South elongated volcanic complex developed along the Aeolian-Tindari-Letojanni Fault (ATLF) (Ruch

* Corresponding author.
E-mail address: matteo.lupi@unige.ch (M. Lupi).

https://doi.org/10.1016/j.jvolgeores.2025.108410
Received 11 October 2024; Received in revised form 27 June 2025; Accepted 9 July 2025
Available online 31 July 2025

et al., 2016) (Fig. 1a). The ATLF is locally fragmented into a complex NNW-SSE right-lateral fault system and it is seismically active (Ventura, 2013; Palano et al., 2015) (Fig. 1a). Foci are generally above 15 km depth (Fig. 1c where the Moho is suggested to occur (Piochi et al., 2009)). The plumbing system of Vulcano is proposed to be a vertically extensive, unstable polybaric domain hosting multiple magmatic reservoirs in a locally ductile (upper) crust (De Astis et al., 2013; Nicotra et al., 2018; Totaro et al., 2022). While the deeper magmatic reservoir of Vulcano is believed to be located at about 20 km depth (Piochi et al., 2009; De Astis et al., 2013; Nicotra et al., 2018) the shallower reservoir is suggested to occur at ~2 km depth (Chiarabba et al., 2004; Blanco-Montenegro et al., 2007; Piochi et al., 2009; De Astis et al., 2013; Nicotra et al., 2018; Cintorrino et al., 2019). A recent magnetotelluric study could not clearly identify such a shallow reservoir. However, the 3D S-wave velocity model obtained by Stumpp et al. (2024) through nodal ambient noise tomography (NANT) shows a low-velocity anomaly (around −40% of relative velocity variation) beneath Vulcanello and La Fossa with a well-defined morphology. Stumpp et al. (2024) show that the region below La Fossa is characterized by low shear wave anomalies at about 1.5 km depth where a prominent subvertical shear wave anomaly is found. The hydrothermal system seats on subvulcanic units and develops from about 1 km depth upwards (Alparone et al., 2010; Stumpp et al., 2024). Stumpp et al. (2024) show a large-scale caldera-like structure and points out the key role of NE-striking faults in promoting unrest. Data from an exploration geothermal well drilled near La Fossa cone (Vu2 bis) show that at about 200 m depth, pressure and temperature are about 18 bars and 200 °C, respectively (Sommaruga, 1984). Assuming a constant geothermal gradient, this implies a transition to ductile rheologies below about 1 km depth, i.e. about the region where we locate the source of the 2021 deformation.

Over historical times, Vulcano featured long periods of rest interrupted by explosive and effusive eruptions (De Astis et al., 2013), the last one being in 1888–1890. Major recent unrests occurred in 1987–90, 1996–98, 2004–05, and 2009 and did not lead to eruptive activity. The unrests have been characterized by shallow micro-seismicity (Alparone et al., 2019) coupled with increased fumarolic activity and significant releases of CO_2 (Chiodini et al., 1996). In September 2021, Vulcano entered a new unrest phase more intense than those of recent decades. Prominent deformation centred in the northern part of Vulcano coincided with the appearance of new fumaroles and the spatial growth of existing fumarolic fields, degassing, temperature rise at the crater rims and geochemical changes of the existing fumaroles. For the first time since the deployment of broadband sensors, swarms of VLP events were recognized on the seismographs (Federico et al., 2023). With the benefit of hindsight, we discovered that Vulcano underwent an unrest with VLP events also in 2018.

Recent studies proposed various hypotheses to explain the 2021 unrest. By using gas measurements (Aiuppa et al., 2022) suggest that the 2021 event was driven by a batch of mafic magma emplaced at about 5 km depth. Geochemical changes have also been measured by Inguaggiato et al. (2022) and Federico et al. (2023), who propose a deep-seated change in the plumbing system of Vulcano. In contrast, Di Traglia et al. (2023) use a combination of geodetic, satellite and seismic data to discuss a hydrothermally-driven unrest. Finally, Stumpp et al. (2024) suggests that either magmatic or tectonic perturbations may destabilize the plumbing system of Vulcano promoting the progressive northwestwards extension of the system that capitalizes on NE-striking lineaments.

By considering a set of seismic, geodetic, and sub-fumarolic ground temperature observations collected over the last decade at Vulcano we provide a multidisciplinary perspective of the 2018 and 2021 unrests. Most of the recent literature focused only on the 2021 unrest, thanks to the availability of large amount of geochemical and geophysical observations (Aiuppa et al., 2022); Inguaggiato et al. (2022); Federico et al. (2023); Di Traglia et al. (2023); (Stissi et al., 2023), so the 2018 unrest passed unnoticed. To fill this gap, we provide an in depth analyses of both unrests, providing also a novel interpretation about their responsible mechanism.

2. Data and results

Our study rely on a multidisciplinary dataset that includes seismic, geodetic and sub-fumarolic ground temperature. Fig. 1b shows the distribution of the used instrumental networks, while a detailed description of each dataset is reported below.

Seismology. The seismic network of Vulcano (Fig. 1) typically records volcano-tectonic and seismo-volcanic events (Alparone et al., 2019). The cross-sections in Fig. 1c, and d show the distribution of seismicity from 2011 to 2022 indicating that seismic events are remarkably shallower in the surroundings of Vulcano (around 30–40 km along profile A-A'). The seismicity NW of Vulcano seems to bound a listric-like structure dipping NW-wards (Fig. 1c). In Vulcano, shallow (< 5 km depth) and deep (> 5 km depth) crustal seismicity is characterized by both low and moderate magnitudes, respectively (Fig. 1). Fig. 2 shows the comparison between crustal (deeper than 5 km depth) and shallow (less than 5 km depth) seismic strain release of earthquakes that occurred over the last decade within a 10 km radius around La Fossa.

Recent unrests at Vulcano are characterized by the occurrence of VLP events that have been discovered in the seismic records for the first time (Federico et al., 2023). The source generating the VLP events has been located at about 1 km depth to the North of La Fossa main crater by Federico et al. (2023). The waveforms and spectra of the VLP events are shown in Fig. 3. A careful re-inspection of the seismic records allowed us to find VLP events also occurring during the unrest of 2018 (Fig. 5c). We observed that both the 2018 and 2021 VLP events have similar waveforms (Fig. 3), with only minor differences in the first pulse, suggesting a common mechanism. To quantify the total number of VLP events, we carried on a manual count of their occurrences (Fig. 4) for the early period of the 2021 unrest. VLPs peaked at 450 and 40 events per day in 2021 and 2018, respectively. In 2021, we notice a long-lasting transient behaviour of the VLPs that is characterized by periods of intense VLP release separated by periods of low activity. Such a spasmodic and transient occurrence of the VLPs lasting several months is well depicted in Figs. 4 and 5e where also a marked and progressive decay of the number of events of each cluster can be recognized. The VLPs sequences that began in June 2018 and September 2021 have been preceded by increases in deep cumulative seismic strain rates of earthquakes in August 2016 and in January 2020, respectively (Fig. 2). Similarly, the shallow (i.e. inside the hydrothermal system) cumulative strain rates of August 2018 and October 2021, followed the June 2018 and September 2021 VLPs sequences, respectively. If interlinked, this sequence of events suggests a deep perturbation, followed by VLP sequences, that in turn lead to shallow microseismicity (Fig. 2).

Geodesy. The geodetic monitoring of Vulcano and Lipari counts 7 continuous GNSS stations (Fig. 1b). We processed the data collected between 2006 and 2022 with the GAMIT/GLOBK packages (Herring et al., 2010). To improve the overall configuration of the network and to provide a robust external global reference frame to tie the regional measurements we included data recorded by 20 global tracking stations (continuously operating) from the EUREF permanent GNSS Network. We used the GLOBK package (Herring et al., 2010) to combine the solutions to estimate a consistent set of daily time-series positions in the ITRF14 reference frame. We investigated each time-series to detect changes in the linear trends, periodic signals and antenna jumps. All time-series were characterized by a linear trend for most of the analysed time intervals. We quantify the 3D long-term velocity field in GLOBK by combining all the daily solutions spanning the 2006–2017 time interval (Table 1). We used this velocity field to set a local reference frame to isolate the ground deformation pattern related to transient episodes.

The procedure points out two significant transients during early 2018 and in 2021 both detectable on the North component of the IVLT station (Fig. 5a). On such a time-series, both the 2018 and 2021 transients show a southwards motion. Yet, by considering the

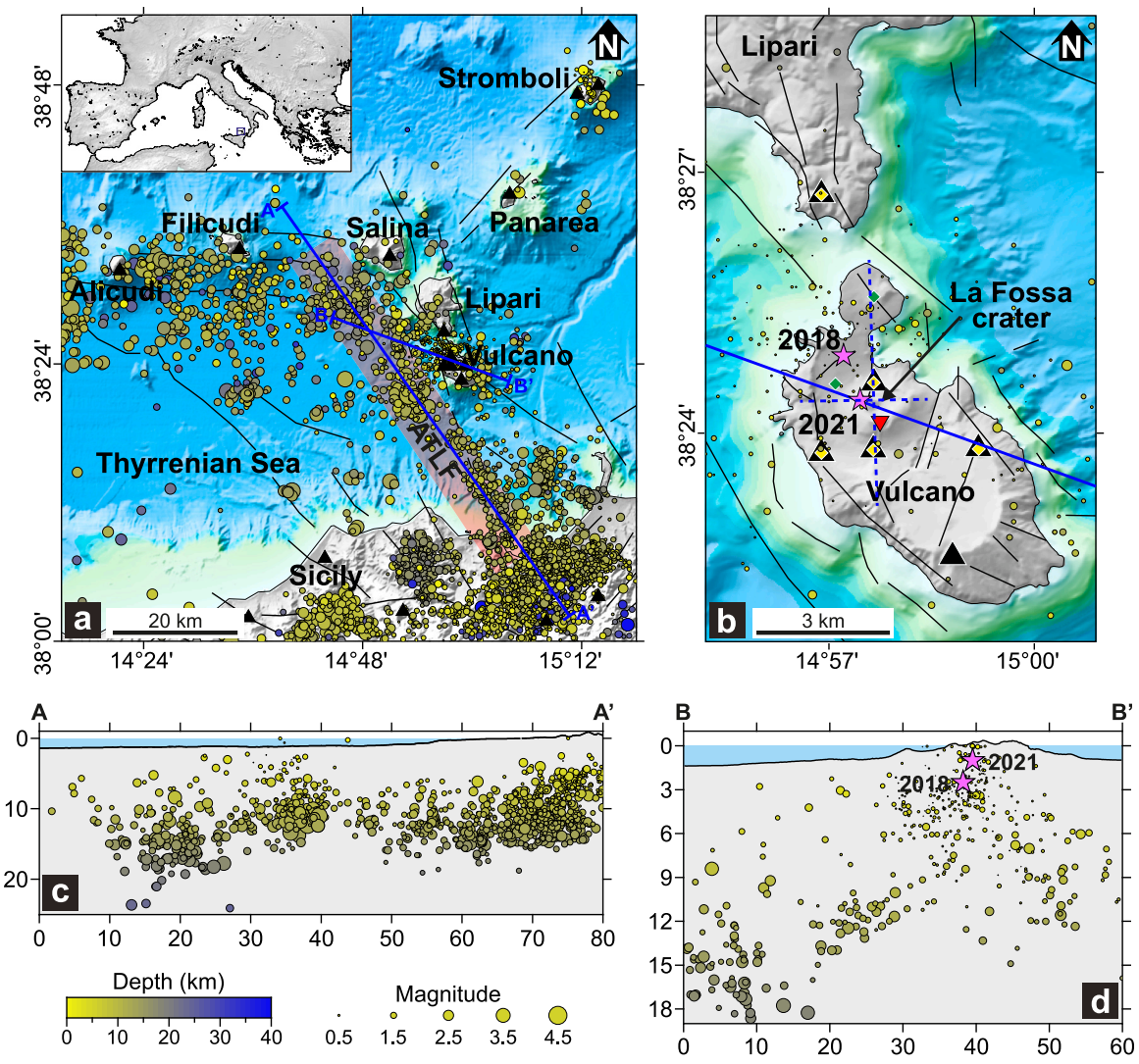

Fig. 1. Seismotectonic maps of the region and distribution of the monitoring network used in the study. (a) Simplified tectonic map of the Aeolian Archipelago and North Sicily. The instrumental seismicity from 2011 to 2022 is shown with circles showing magnitude and depth. Major faults are shown as black lines while the seismic stations are reported as black triangles. The red transparent band shows the deformation region of the Aeolian-Tindari-Letojanni Fault. A-A' and B-B' are the cross sections shown in panels c and d, respectively. The seismicity plotted in the figure is taken from (Alparone et al., 2019) and Barberi et al. (2020). (b) close up around Vulcano. Seismic stations, GNSS stations and the thermal probe are reported as black triangles, green diamonds and red triangle, respectively. The blue stars stand for the 2018 and 2021 modelled pressure sources. (c) A-A' cross-section showing earthquakes projected within ±3 km from the profile. (d) B-B' cross-section showing earthquakes projected within ±3 km from the profile. Stars indicate the positions of the modelled sources for the 2018 and 2021 unrests.

Table 1
Site id, coordinates and long term linear trend (with associated uncertainties) of all the GNSS stations used to set the local reference frame. East, North and Up values are in mm/year.

Site	Long	Lat	East ± σ	North ± σ	Up ± σ
IVCR	14.961	38.410	22.62 ± 0.09	22.37 ± 0.25	−8.54 ± 0.26
IVGP	14.961	38.39	22.24 ± 0.13	24.04 ± 0.13	−5.52 ± 0.34
IVLT	14.948	38.396	23.14 ± 0.11	24.49 ± 0.08	−6.17 ± 0.22
IVUG	14.986	38.397	21.53 ± 0.09	24.46 ± 0.10	−4.56 ± 0.21
VCSP	14.952	38.409	24.22 ± 0.10	21.56 ± 0.09	−9.56 ± 0.13
VVLC	14.961	38.426	20.78 ± 0.55	22.13 ± 0.15	−6.85 ± 0.61

displacement field of the whole geodetic network solution (Fig. 6), each transient is related to an island-scale inflation episode, suggesting a pressurization of the plumbing system of Vulcano.

Both displacement fields show a similar pattern, with the one related to the 2021 transient characterized by values larger than those observed during the 2018 transient. Despite the sparse distribution of the GNSS stations, the agreement between the 2021 and 2018 is consistent. The overall network geometry changed during the two observed inflation episodes, especially on its northern sector, mainly due to temporary malfunction of some stations. For each unrest, at least a station is always working on this sector of the volcano, providing a useful constraint on the overall deformation field. The displacement fields have been used to constrain isotropic elastic half-space inversion models. We adopted a same inversion strategy for both unrest episodes, in order to achieve a set of robust model parameters and to allow an easy comparison between the modelled sources. A volcanic unrest is generally related to either a magmatic intrusion along an uprising dike or to the pressurization of part of the plumbing system, e.g. Dzurisin (2006). Expected deformation patterns at the surface related to any of these two sources are similar, although an homogeneous and radial pattern is more typical of hydrothermal pressurization. In our case, the measured deformation pattern suggests the activation of a pressurization source. Due to the limited number of available GNSS observations sampling during the two unrest episodes, we considered the simple analytical formulation described in Mogi (1958). Despite its

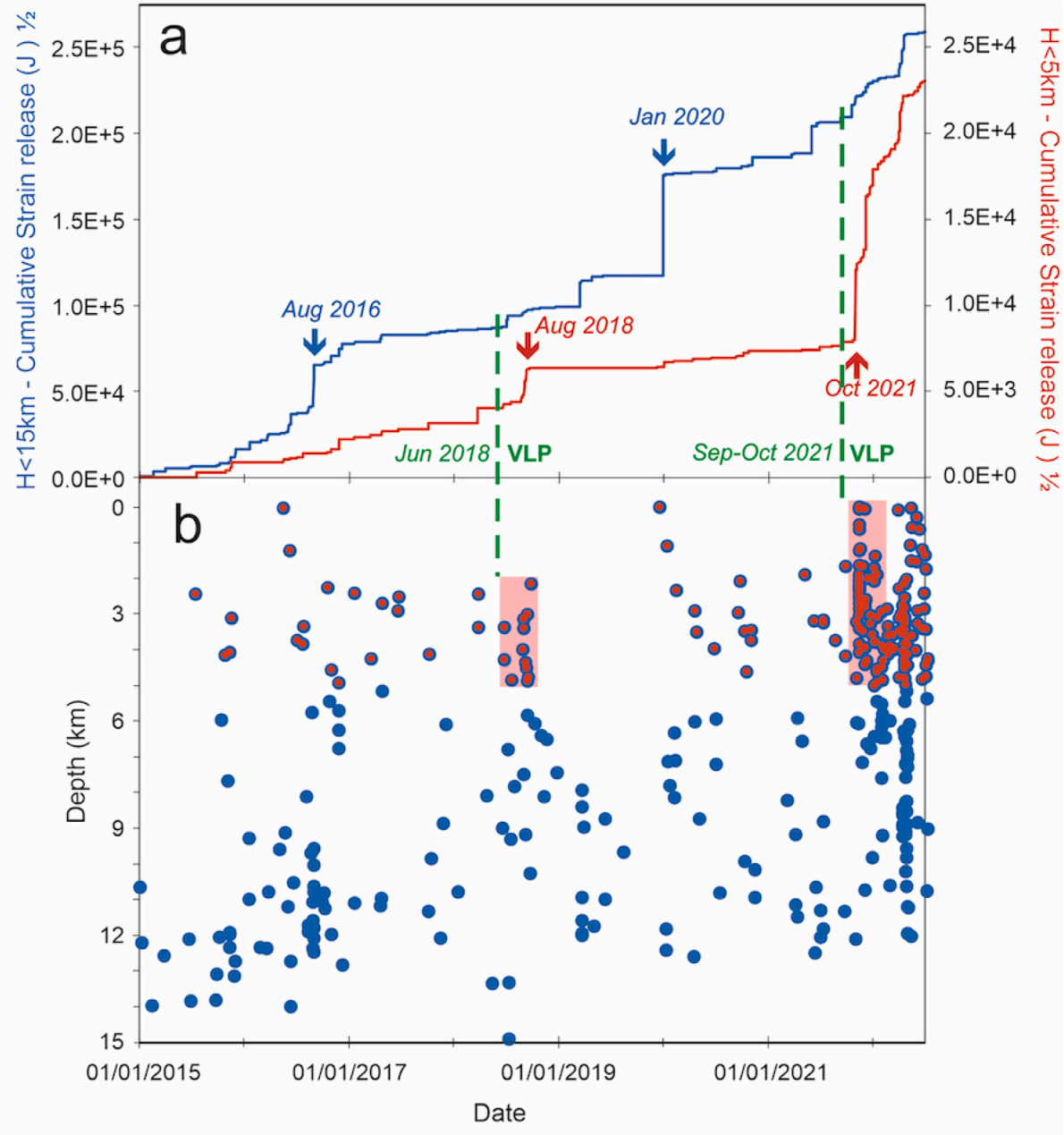

Fig. 2. Temporal evolution of cumulative seismic strain rate. Seismic energy (E) is computed using the relationship $logE = 9.9+1.9M - 0.024M^2$ (Richter, 1958) where M is the value of the magnitude associated with the earthquake. The solid blue and red lines show the temporal evolution of the cumulative seismic strain release from 2015 to 2024 for deep (<15 km) and shallow earthquakes (<5 km) within a 10 km radius around la Fossa, respectively. For both the 2018 and 2021 unrests the temporal evolution begins with deep seismic events, followed by the appearance of VLP events (green dashed vertical lines) that are then followed by shallow microseismicity located in the hydrothermal system. b) Depth distribution of the seismicity (blue dots with depth less than 15 km) and shallow earthquakes (the red dots with depth less than 5 km).

computational simplicity, such an analytical formulation is largely used for interpreting surface deformation fields in a variety of geological problems (Dzurisin, 2006). We therefore assumed a Mogi source embedded in a homogeneous, isotropic, Poisson-solid half-space domain characterized by a shear modulus of 30 GPa. The inversion procedure was performed by using a genetic algorithm approach (Tiampo et al., 2000). Both horizontal and vertical GNSS components, estimated for each unrest episode have been inverted by taking into account a weight proportional to the estimated displacement errors. The model fit was evaluated by means of the root mean square error (RMSE) that quantifies the absolute fit of the model's predicted values to the observed data (the lower the values of RMSE, the better the fit). This is computed as:

$$RMSE = \sqrt{\sum_{i=1}^{n}((P_i - O_i)^2)N^{-1}}$$

where N indicates the number of datasets, and O_i and P_i represent the observed and predicted values, respectively.

The best-fit solutions (Fig. 6) indicate a source located at about 2.3 km (positive volume variation of about 0.5×10^6 m^3) and 1.3 km (positive volume variation of about 0.3×10^6 m^3) depth for the unrests of 2018 and 2021, respectively. Table 2 shows the summary of the located sources. The uncertainties of the best fitting parameters for each modelled source were estimated by adopting a Jackknife resampling

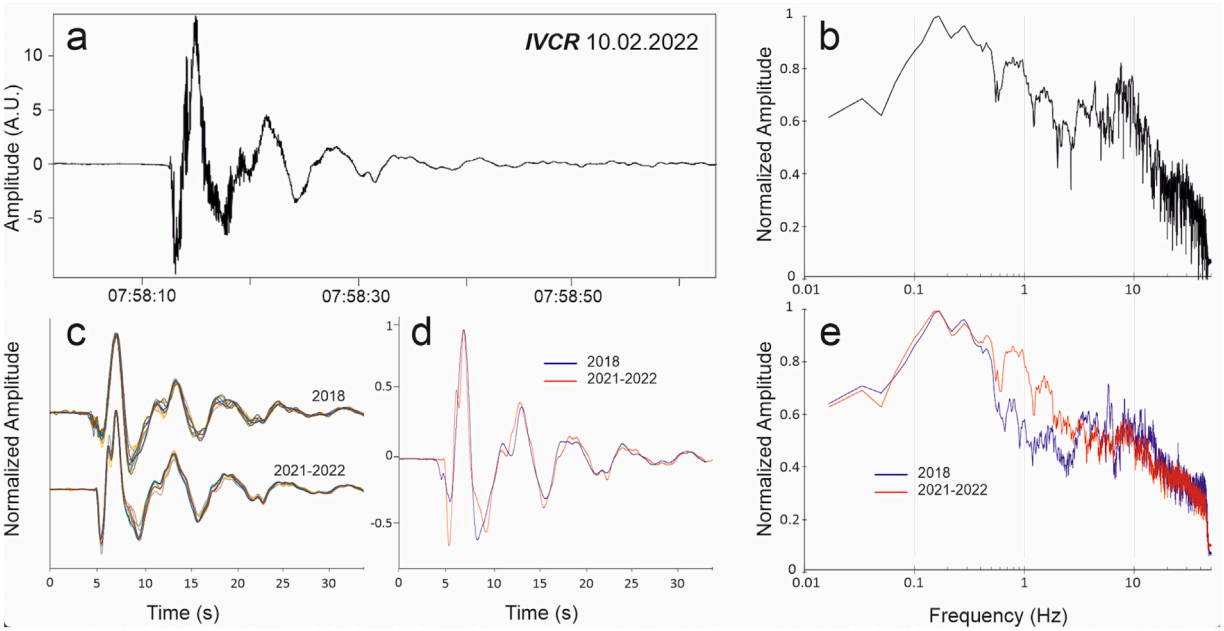

Fig. 3. Waveforms and spectral distribution of representative VLP events. (a) waveform of the most energetic VLP event recorded in the period 2018–2022, 10 February 2022 at 07:58 UTC and (b) its spectrum; (c) normalized waveforms of eight higher amplitude VLP events recorded during 2018 and 2021–2022, respectively; (d) stacking of the waveforms of the VLP signals reported in C for both periods; (e) average spectrum for the 2018 and 2021–2022 related to VLP signals of Fig. 3c.

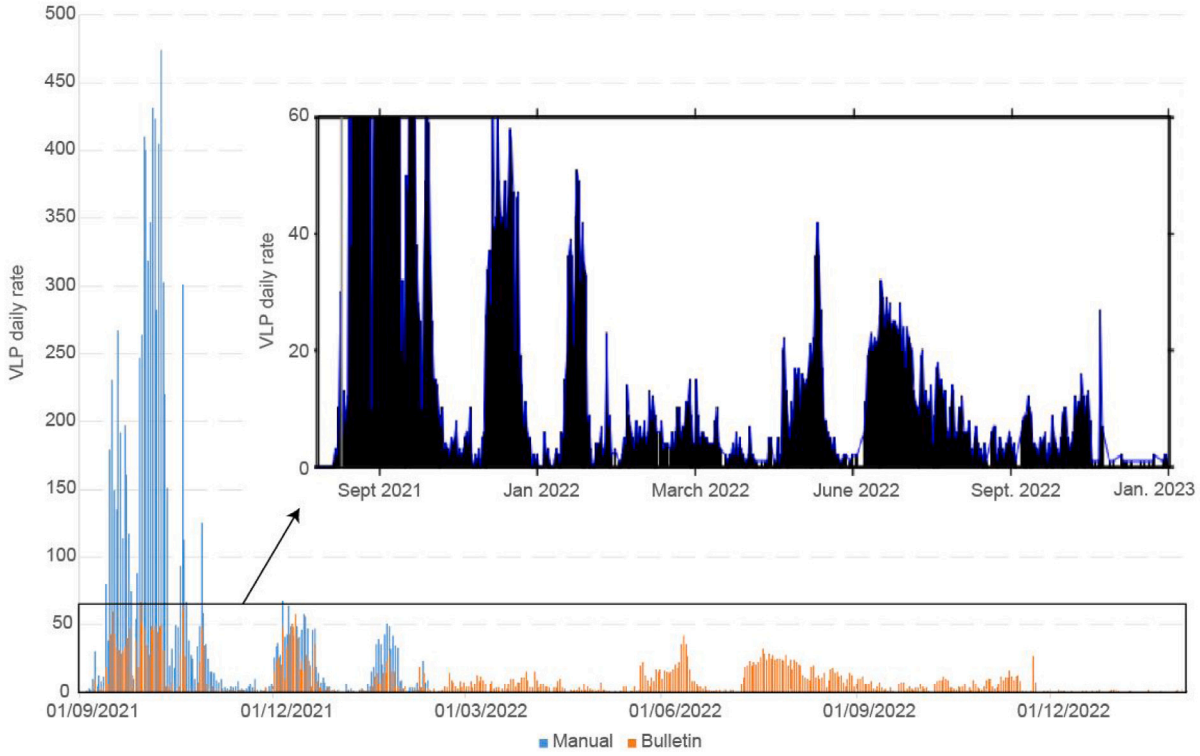

Fig. 4. Evolution of VLP daily rate from 2021 to 2022. The light blue colourbars show the events identified manually and in orange, the ones automatically detected and reported in the INGV bulletin catalog. The close up show by means of a saturated scale the transient and spasmodic character of the sequences.

method (Efron, 1982). This method is largely used for assessing the bias and standard error in a statistical estimation problem. Jackknife resampling method systematically recomputes statistics a large number of times leaving out one observation (or a group of observations) at a time from the initial dataset. This implies that only a set of new inversions starting around the best solution are carried out each time. The variance of the statistic (σ) is calculated as:

$$\sigma = \sqrt{((n-1)n^{-1}) \sum_{i=1}^{n} (q_i - q_m)^2} \quad (1)$$

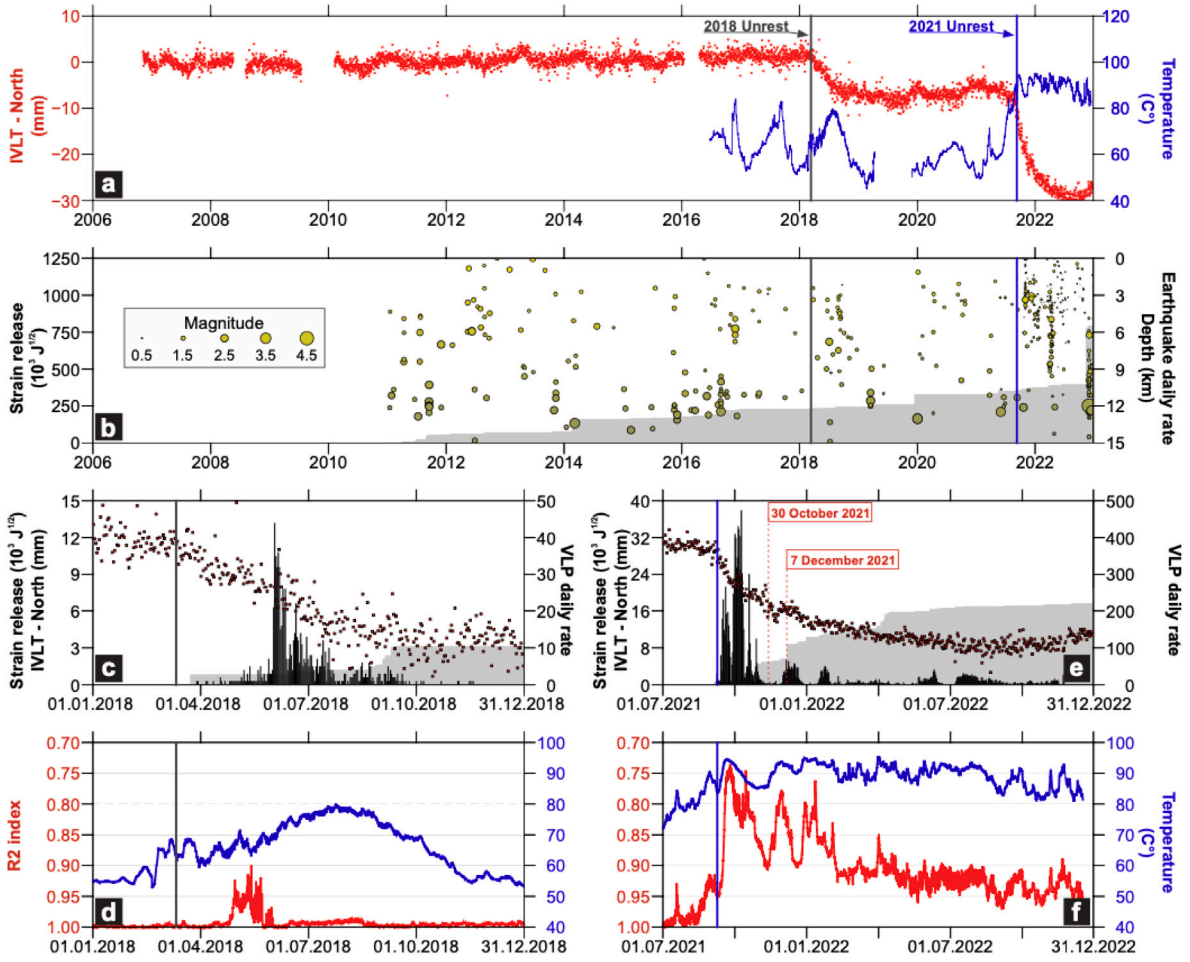

Fig. 5. Geodetic, seismic and temperature time-series used in the study. (a) North component (red points) of the station IVLT (see Fig. 1b for its position) showing two transient events in 2018 and 2021 (marked by the two vertical lines). The temperature time-series recorded at the top of La Fossa cone at 70 cm depth is also reported in blue. The temperature, climbs up before the unrest, in particular for the 2021 event. (b) The seismicity (depth ⩽ 15 km) occurred in a radius of 10 km from La Fossa cone at 70 cm depth is reported as circles. The cumulative seismic strain release is reported as a grey area. (c) Time series of (i) seismic strain release (grey area) of shallows earthquakes (depth ⩽ 5 km) occurred in a radius of 10 km from La Fossa cone, (ii) daily number of VLP events (black histograms) and (iii) North component of the station IVLT (red points) during the 2018 unrest. (d) Time-series of the R^2 index (red line) and temperature at 70 cm depth (blue line) during the 2018 unrest. (e) Time series of (i) strain release (grey area) of shallows earthquakes (depth ⩽ 5 km) occurred in a radius of 10 km from La Fossa cone, (ii) daily number of VLP events (black histograms) and (iii) North component of the station IVLT (red points) during the 2021 unrest. (f) time-series of the R^2 index (red line) and temperature at 70 cm depth (blue line) during the 2018 unrest. Note that the figure shows a combined counting of the VLP events, i.e. manually counted (for 2018 and until February 2022) and extracted from the reports for the rest. This is detailed in Figure S2 in the supplemental online material.

Table 2
Parameters of the modelled sources. Coordinates are in UTM 33N projection.

Parameters	2018 Unrest	2021 Unrest
Easting (km)	495.951 ± 0.251	496.301 ± 0.145
Northing (km)	4251.828 ± 0.115	4250.888 ± 0.112
Depth (m)	−2267±0129	−1308 ± 96
ΔV (m^3)	0.53 ± 0.05	0.34 ± 0.03
RMSE	4.1	7.3

where q_i is the value of the source parameter in the i^{-th} inversion, q_m is the mean of all the n parameter values and n is the number of observations. Estimated uncertainties for each parameter are also reported in Table 2.

Temperature. The temperature monitoring station used in this study consists of 4 probes reaching 10, 30, 50, and 70 cm depth installed in a sub-fumarolic area located on the inner southern rim of La Fossa cone (Fig. 1, (Ricci et al., 2015)). Over the years the probes recorded temperature variations and changes in the coefficient of determination R^2 (Ricci et al., 2015; Gaudin et al., 2017) allowing the identification of transient variations in the heat transfer mechanism. A reduction of the R^2 coefficient indicates a transient change from conductive-dominated heat transfer towards advection/convection conditions. Figs. 5e, f show that temperature and R^2 changes anticipate the 2018 and 2021 seismic swarms of VLPs. However, while temperature variations can be affected by external parameters such as seasonal and daily variations, R^2 represents an excellent filter able to reveal endogenous-driven variations. The INGV reports (available at the link: https://cme.ingv.it/bollettini-e-comunicati/bollettini-ingv-vulcano) also indicate that CO_2 increases seem to occur before VLPs.

3. Discussion

The inversion of the 2018 and 2021 geodetic data suggests two sources located at about 2.3 km and 1.3 km depth, respectively (Fig. 6). Both sources inverted from the geodetic data (Fig. 6) are compatible with a pressurization of the volcanic system and based on their location, and given their estimated uncertainties (Table 2) they are statistically considered as two distinct sources. Our estimated uncertainties are generally larger than those reported by Stissi et al. (2023) and Di Traglia et al. (2023), both focusing on the 2021 unrest using different methods for uncertainty estimation. This suggests that the Jackknife

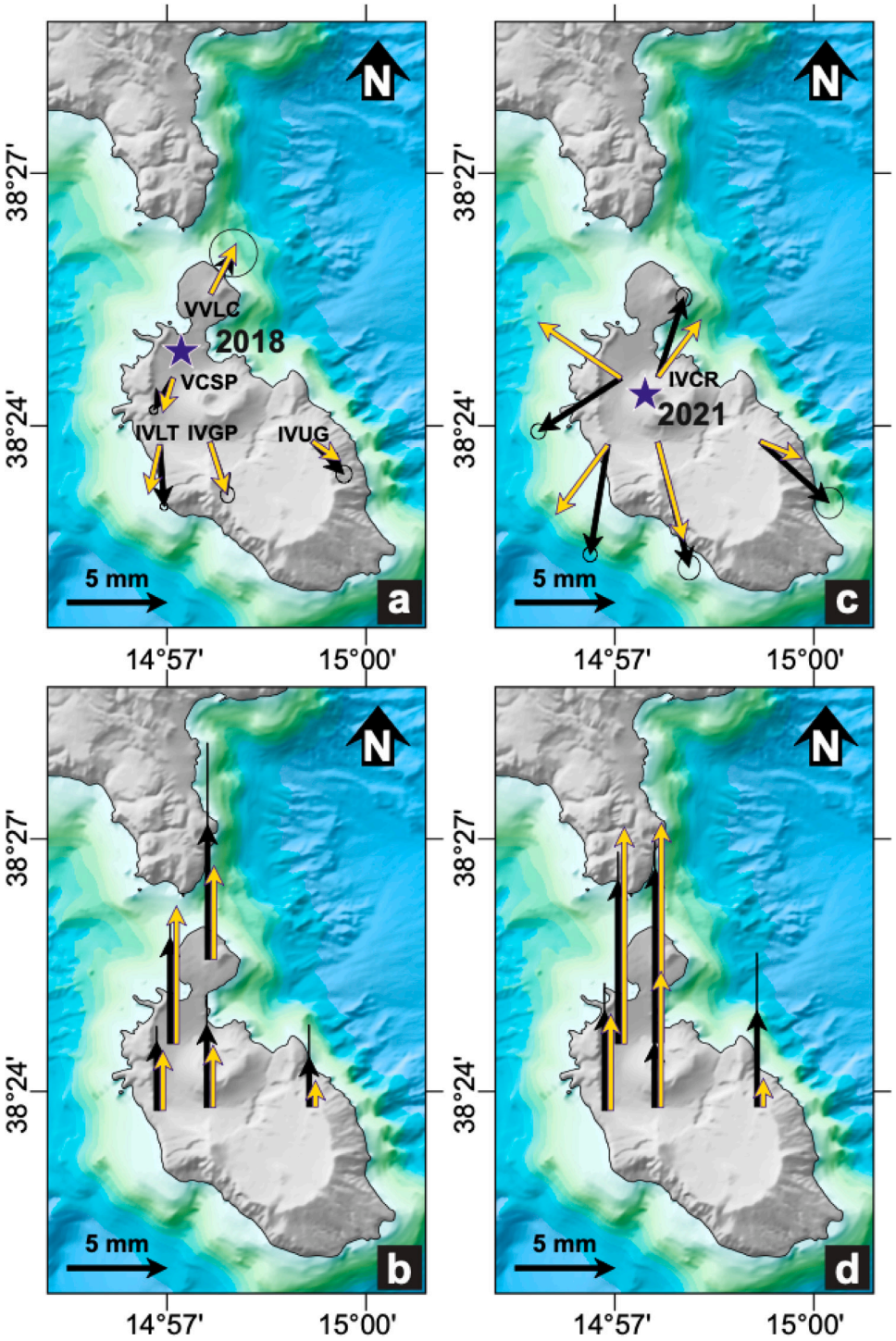

Fig. 6. Proposed locations of the sources driving the geodetic deformations. Observed (black arrows) and modelled (yellow arrows) displacement patterns for the 2018 and 2021 events. The two modelled sources are reported as blue stars. The top and bottom rows show the horizontal and vertical displacements, respectively.

resampling method yields a more conservative estimate of uncertainty. Given this characteristic, the spatial separation between the 2018 and 2021 sources can be considered robust.

To further test whether the 2018 and 2021 unrest episodes were driven by distinct sources, we performed a new inversion for each event using only the four stations common to both periods (VCSP, IVLT, IVGP, IVUG; Fig. 6). Although these results are less well constrained, they show that the spatial separation between the two sources increases to approximately 2.1 km, with the 2018 source being consistently deeper. Both sources are also shifted about 0.9 km northwest of their best-fit locations (Table 2), likely reflecting the limited GNSS coverage in the northern sector of the volcano. Despite these limitations, this simple test supports the conclusion that the 2018 and 2021 unrest episodes were caused by different pressurizing sources. The 2021 source seats below the epicentral depth of the VLP events (Federico et al., 2023). Such a source also partially overlaps with the one derived from the inversion of the geodetic data collected during the 2 September–13 October 2021 time interval (Stissi et al., 2023). It is also below the source derived from the inversion of InSAR data spanning the 15 July–18 December 2021 period (Di Traglia et al., 2023). Despite the different

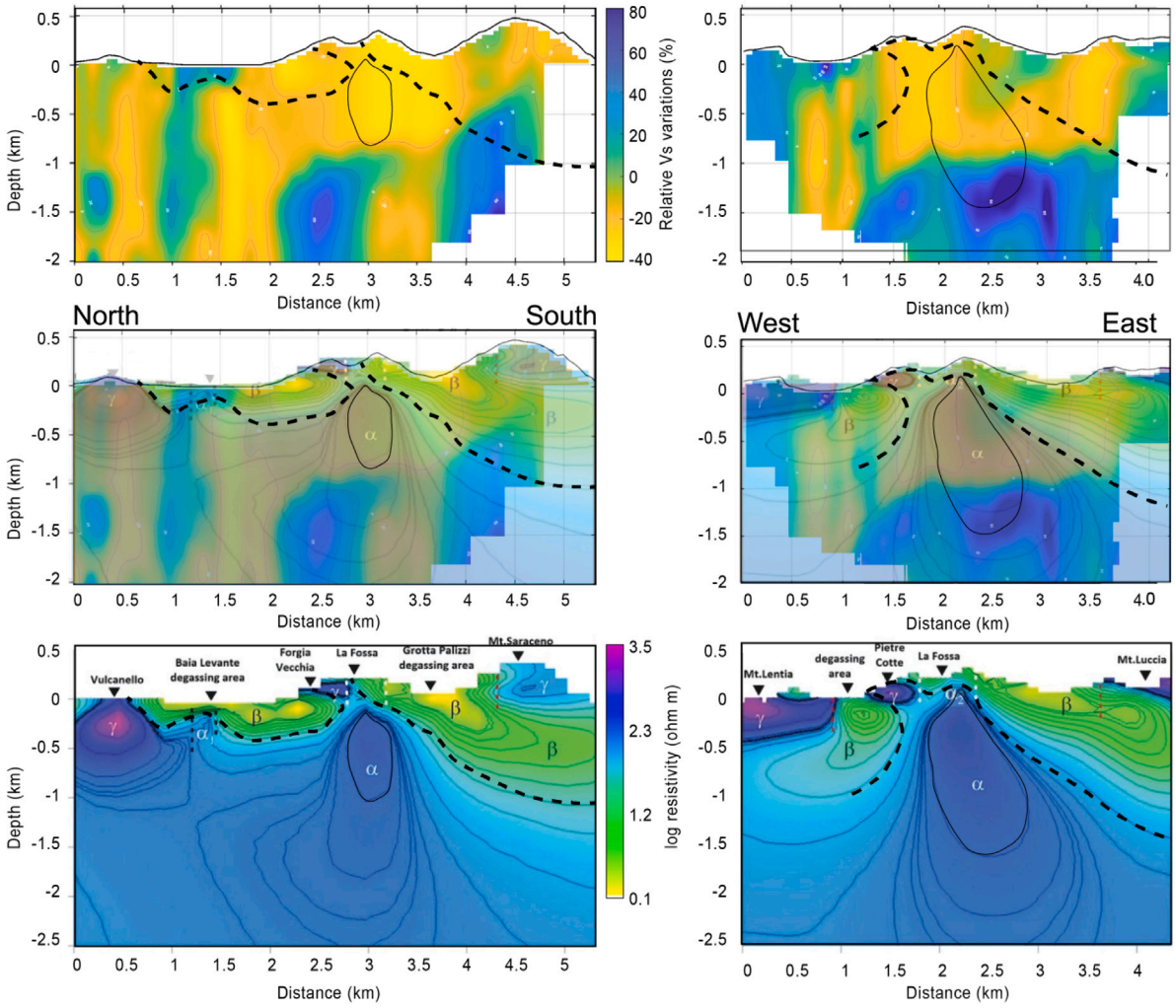

Fig. 7. Comparison between the shear wave velocity and the resistive structure of Vulcano. The top, central, and bottom rows show the NANT data of Stumpp et al. (2024), an overlap between NANT and MT data, and the resistive structure retrieved by Di Giuseppe et al. (2023), respectively. The strike of the profiles is shown by the black dashed lines in Fig. 8a. We notice a good agreement between the two inversions. The thick dashed line reported across the panels represent the transition between conductive and more resistive domains in the bottom row. However, the NANT of Stumpp et al. (2024) provides much higher resolution at depth if compared to the MT data. The MT data of Di Giuseppe et al. (2023) show that the resistive domain intrudes into the conductive domain below La Fossa bulging until about 200 b.s.l.). This corresponds in the NANT data to a region characterized by particularly low Vs anomalies. The MT data are taken from (Di Giuseppe et al., 2023).

time intervals considered, we observe that the pressurization of the system drastically increases since 5–6 September up to mid-October 2021, decelerating in the following months. This is documented by the time series of the continuous GNSS stations located far from the La Fossa cone (see the IVLT north component in Fig. 5). Conversely, InSAR data densely covering La Fossa cone were able to capture surface deformation since early August 2021. Inversions performed on such different datasets spanning across various time intervals show similar results. The sources suggested by Di Traglia et al. (2023) and Stissi et al. (2023) are located at a depth of about 600–800 m, and by considering their geometric shape (and associated model parameters) they define a subvertical elongated region within the 0–1.5 km b.s.l. depth range. Our modelled source (Table 2) partially overlaps with the deeper portion of this elongated region. Our source of the 2018 unrest falls northwards compared to the source of the 2021 event (Fig. 6). The 2018 unrest passed unnoticed before this study mainly because of the lack of significant variations in the parameters generally used for the monitoring purposes. In particular, the seismic network was not calibrated to identify VLPs. By looking at geophysical signals reported in Fig. 5, the 2018 unrest was short-lived and less prominent in comparison to the 2021 episode. This may explain the differences in SO_2 observed by Aiuppa et al. (2022). In fact, Inguaggiato et al. (2022) show that the max SO_2 values recorded in 2016, 2018 and 2019 peak to about 50 tons/day compared to the 143 ± 60 tons/day reported by Aiuppa et al. (2022) for the 2021 event. A clear difference with respect to the 2021 unrest is given by the significant temporal delay between the starting of temperature increase (February 2018), the onset of ground deformation (late March 2018), a reduction of the R2 coefficient (late April 2018) and the increase of VLP events occurrence (May 2018) (Fig. 5). The long-term temperature time series reported in Fig. 5, is related to a common seasonal pattern instead of endogenous-related dynamics. The inversion of geodetic data infer a 2018 pressurizing source characterized by a positive volume variation of about 0.5×10^6 m^3 and located at a depth of 2.3 km b.s.l. beneath the inhabited area of Vulcano Porto (Fig. 6). This source is different from the one inferred for the 2021 unrest. However, both sources could be compatible with the rise of exolved fluids/brines from a deeper source, along a NE-striking and north-west dipping fracture-like pathway as suggested by Stumpp et al. (2024).

When comparing the shear wave anomaly distribution of Stumpp et al. (2024) against the MT data produced by Di Giuseppe et al. (2023) we notice that MT data broadly correspond to regions of low shear wave anomalies (Figs. 7, 8a show the direction of the profiles). The Nodal Ambient Noise Tomography (NANT) of Stumpp et al. (2024)

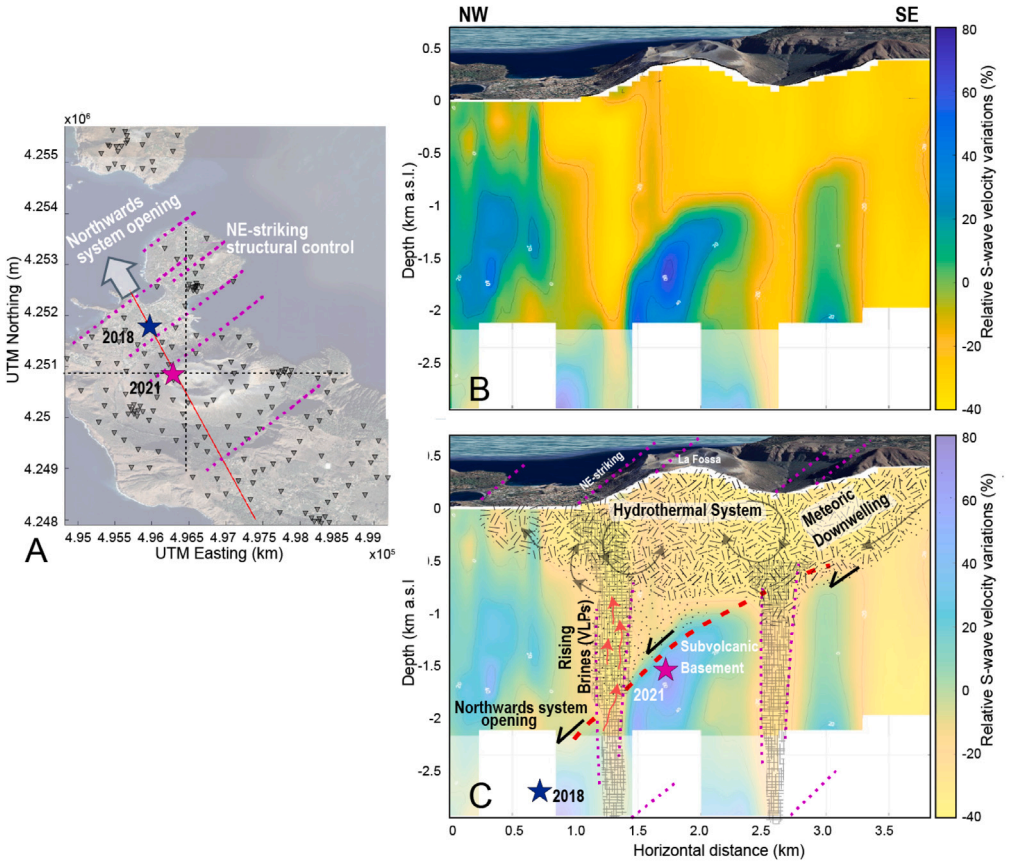

Fig. 8. Conceptual showing the shear wave anomalies beneath Vulcano. The anomalies are extracted from the S-wave velocity model of Stumpp et al. (2024). Prominent S-wave velocity anomalies point out a sub-vertical magmatic system where brines rise generating VLPs. The horizontal shaded domain below 2 km depth has less reliable resolution according to Stumpp et al. (2024). The location of the VLP events shown by Federico et al. (2023) coincides with the low shear wave anomaly below la Fossa crater. Similarly, we identify a region of low shear waves just below Baia di Levante (Fig. 7 N-S profile), that is a region characterized by intense degassing during the 2021 unrest (Federico et al., 2023).

clearly show the complex subvolcanic domain of Vulcano indicated by faster anomalies. Its fragmentation into sub-vertical structures is possibly linked according to Stumpp et al. (2024) to NE-striking normal faults accommodating the northwards migration of the volcanic complex (Fig. 8).

Fig. 7 shows that MT data have little variation and Di Giuseppe et al. (2023) state that several parameters affect the spatial uncertainty distribution of resistivity models. This hinders the ability to resolve high-resistivity features when overlaid by low-resistivity anomalies. This is particularly the case when the base of such anomalies is poorly constrained like in Vulcano. However, this is a typical limitation of MT models that are typically not capable of penetration under the clay-cap layer and reveal an adequate resolution at depth. However, geothermal in volcanic systems are still primarily being investigated with MT methods. Fig. 7 clearly show that MT and NANT are complementary methods, with MT being able to resolve the shallow portion of the system and hint on the resistive domain. Vice-versa, NANT data struggle in the shallow domain but perform greatly at depth where the plumbing system is developed. This makes NANT an ideal tool to investigate volcanic and geothermal systems that soon will be deployed as much as MT.

Understanding what may cause volcanic unrests has major societal implications, both for present and future risk mitigation plans. Certainly, high-resolution tomographies may help understanding the driving mechanisms of volcanic crises. During the 21st century several volcanic unrests occurred worldwide, and about 1/3rd of them did not result into an eruption (Phillipson et al., 2013). For instance, this was the case with volcanoes such as Tangkubanparahu, Cotopaxi, Deception Island, Irazu, Taal, and Karkar (Pritchard et al., 2019). Volcanic unrest can consist of disruptions over years in several parameters such as fumarolic activity, thermal anomaly, deformation, and seismic activity. Some volcanoes are well known for their period of unrest, such as the recent 2019 unrest period of Taupo (Illsley-Kemp et al., 2021), or the succession of unrest periods (*bradiseismic crises*) at Campi Flegrei, in 1969–1972, 1982–84, including the ongoing unrest (e.g. Iervolino et al. (2024). Currently, Campi Flegrei is being affected by an exacerbation of values of the monitoring parameters but still the causative drivers of such an event are not clear. Such an incertitude is something widely occurring at volcanoes and studies like ours may help understanding some of the processes occurring at depth. Vulcano's unrests have been (suggested to be) driven by hydrothermal activity (Ricci et al., 2015; Selva et al., 2020). More recently, alternative interpretations have been proposed to explain the 2021 unrest. Aiuppa et al. (2022) suggest that the volcanic crisis was caused by the intrusion of a melt at about 5 km depth while (Di Traglia et al., 2023) suggest that the inflation was caused by the passing of fluids across geological structures. We argue that both options may be viable but the transient character of the VLPs suggest a tectonic control modulating the release of fluids. A well establish conceptual model that could accommodate the spasmodic nature of VLP events (Fig. 4) is the fault-valve behaviour proposed by e.g. Sibson (1990), Graham (2011). This would also be in agreement with the magmato-tectonic mechanism proposed by Stumpp et al. (2024) to explain the 2021 unrest. We exclude the emplacement of a dike in the shallow plumbing system since dike emplacements are not often associated to VLP sequences lasting several months (e.g. Ágústsdóttir et al. 2016). Additionally, during dike emplacement, microseismicity is rather characterized by double-couple solutions progressing towards the direction

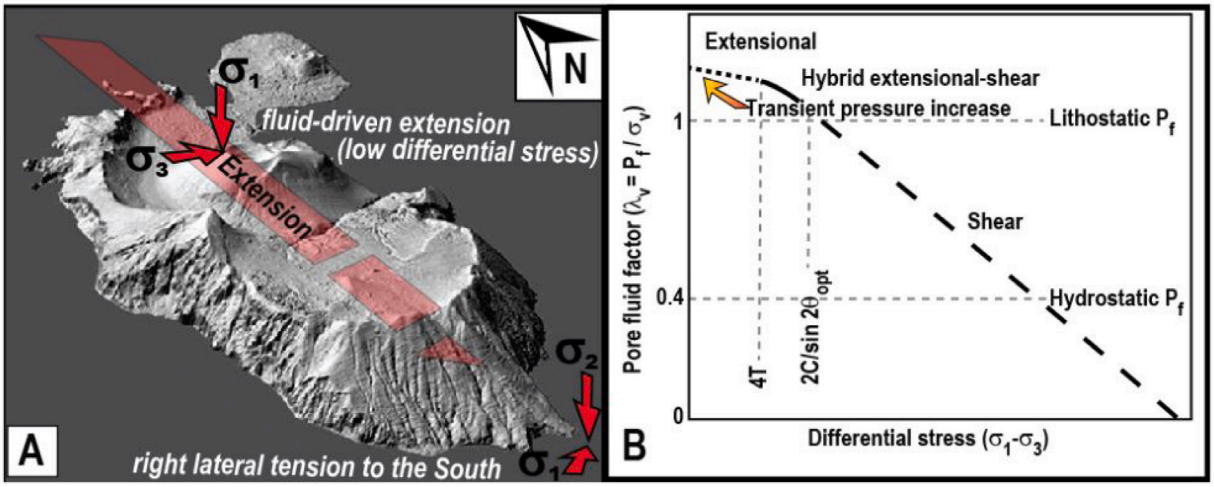

Fig. 9. Tectonic and geomechanical model of Vulcano. (Ruch et al., 2016) suggest that the active part of Vulcano is driven by extensional tectonics. To the South, the dominant regime is strike slip (in agreement with the kinematics of the Aeolian-Tindari-Letojanni fault). (b) When the differential stress is reduced because of deep-rising brines, it is possible to locally transit into an extensional regime that may be able to accommodate the lithostatic pressure from depth. T is the tensile strength, C the cohesive strength and θ is the angle at which a given fault is oriented to σ_1. The conceptual model is modified from (Cox, 2010).

of opening of the fracture (Woods et al., 2019). Dike-driven unrests cause a marked microseismicity that is broadly synchronous with the emplacement of the magma at depth. For instance, microseismic events caused by the Bárðarbunga intrusion, Iceland, lasted less than a few weeks (Ágústsdóttir et al., 2016). Seismicity triggered by dike intrusions at rift margins lasts up to a few months (Cesca et al., 2022). No sign of progressing microseismicity has been shown in the literature so far for what concerns both the 2018 and 2021 Vulcano unrests.

During the 2021 unrest, seismic activity at Vulcano spanned more than a year and VLP events decreased in December 2022 and resumed in June 2024. Figs. 4, 5e show the transient nature of VLP seismic sequences. Interestingly, VLP occur in clusters of events separated by seismically quiescent periods. Such a transient behaviour is often associated with discrete releases of over-pressure through seismic sequences, that is not compatible with a hydrothermal causative source for the 2021 event. While we also favour a fluid-driven mechanism, we notice that hydrothermal fluids (i.e. a mix of shallow groundwater, percolating seawater and fluids exolved from the magma) may be confined in the upper part of the conduit. We argue that if VLP events are associated to hydrothermal circulation, even if more prominent during the 2021 unrest, VLP events should have been found in the seismic records before. This is not the case and the only other period characterized by VLP events at Vulcano, since the deployment of the broadband network in 2005, was the 2018 (unnoticed) unrest that had a much deeper source.

The 3D S-wave velocity model obtained by Stumpp et al. (2024) with data collected during the 2021 unrest suggests that NE-striking fault systems could have a key role in modulating the unrests of Vulcano and the associated seismic activity. Fig. 8 (interpretation in panel C) confines the hydrothermal convection cells in the upper part of the volcanic system. Well data show that temperature at 200 m depth is as high as 200 °C (Sommaruga, 1984). Interestingly, Stumpp et al. (2024) show a northwards propagation of the plumbing system are regions of low shear wave anomalies below La Fossa (Fig. 8b) that well correspond to the position of the VLP events located by Federico et al. (2023). All the geodetic data inverted to constrain the source of deformation driving the 2021 unrest (Di Traglia et al., 2023; Stissi et al., 2023), including this study, concur in suggesting a near radial extensional pattern. As previously mentioned, such a pattern appears related to the activation of a pressurizing source instead of the intrusion of a magmatic dike. Moreover, a dike intrusion would be also not fully compatible with the seismicity recorded in Vulcano, while the discharge and rise along these conduits of hot brines (Fig. 8c) at near-lithostatic pressure into the base of the hydrothermal system may effectively cause VLP seismicity. The transient release of VLP series shown in Fig. 4 suggests a potential spasmodic pressure release. The occurrence of transient fluid releases is an established concept departing from the initial model of fault valve behaviour first introduced by Sibson (1990) for brittle rheology. The model was then adapted to a variety of geological settings to explain over-pressure release across ductile (Fournier, 1999) and brittle (Miller and Nur, 2000; Graham, 2011) domains. This concept is adapted to Vulcano in Fig. 9. Vulcano sits upon the Aeolian-Tindari-Letojanni strike slip fault system (Fig. 1a). Ruch et al. (2016) suggest that this lateral regime becomes extensional in the Northern part of Vulcano (Fig. 9a). Such a proposition is also supported by the high-resolution NANT of Stumpp et al. (2024) who point out how the interaction between magmatic and tectonic processes may be responsible for the unrests of Vulcano. In fact, normal faulting is suggested to act like an incipient N-striking local rifting in connecting Vulcano and Lipari volcanoes (Ruch et al., 2016) (Fig. 8a). Overpressured fluids focus where NE-striking faults intercept the northwards extension capitalizing on regions of enhanced hydraulic transmissivity. Here, at the junction of fault systems the tensile strength of the upper crust is weaker than the surrounding regions and upwell of brines can occur promoting the development of subvertical conduits (Fig. 8c) facilitated by the local change of regime from strike slip to extension (Fig. 9). The release of near-lithostatic pressures at the base of the hydrothermal system, not only compels with the transient character of VLP sequences, but also accommodates the transition from the regional scale strike slip regime into the extension that characterizes the rifting between Vulcano and Lipari. When the vertical lithostatic load is overcame by the fluid pressure at the base of the hydrothermal systems, fluids are released and opening is promoted transiently. In fact, Cox (2010) suggest that at low confining pressures, minor pore pressure changes (for instance caused by rising hot fluids in this case) would facilitate the transition from a shear-dominated to an extensional regime (Fig. 9b). Interestingly, data show that before VLPs series begin, the temperature increases and the R^2 coefficient decreases simultaneously (Fig. 5). Note that in Fig. 5f R^2 and temperature also swing on a similar wavelength in the early time after unrest (i.e. after September 2021) (Harris and Maciejewski, 2000; Christenson et al., 2010). The temperature variations that occurred before the 2018 VLP seismicity increase are likely due to rain events, typical of the Spring season at the Aeolian islands. The temperature increase during spring follows the classic pattern of seasonal variations. The R^2 filters these changes and it has to be noted that the 2018 and 2021 VLP seismic

records differ by one order of magnitude (i.e. VLPs peaked at 450 and 40 events per day in 2021 and 2018, respectively). This suggests that the hydrothermal system is transiently heated up thanks to the contribution of hotter masses, that necessarily have to come from depth. Such rising hot transient fluids are compatible with the radial extension shown by our geodetic data and those of previous authors (e.g. Di Traglia et al. 2023, Stissi et al. 2023). In our conceptual model, the increase of permeability in the shallower crust beneath Vulcano and Lipari, allows the rising of hot fluids which spasmodically release magmatic brines at near-lithostatic pressures. When such brines reach the base of the hydrothermal system, they accelerate (because of decompression) generating the observed VLP events. H_2O and CO_2 separate and pressurize the hydrothermal system causing the observed shallow microseismicity and the extensional deformation observed by geodetic data (Fig. 6). Meanwhile SO_2 precipitates sealing the system preparing the mechanic conditions for the next shallow pressure build up (i.e. transient deformation) (Harris and Maciejewski, 2000; Christenson et al., 2010). Such a model well explains both the 2018 and 2021 unrests, highlighting the progressive rising of hot brines along preferred pathways. While the driving process of the 2018 and 2021 unrest is the same, our geodetic data indicate that the position of the causative source is transient across the plumbing system.

During the 2018 unrest, the temporal shift between the onset of ground deformation and the occurrence of VLP events would be indicative of the time required by the brines to move from the pressurizing magmatic source (2.3 km) up to the base of the hydrothermal system (e.g. 1 km). During the 2021 unrest, such a time has been drastically reduced, being the pressurizing source shallower and located at the base of the hydrothermal system. We remark that a model supporting hydrothermal-driven unrest as postulated by previous studies struggles in explaining the occurrence of newly identified VLPs that should have recorded at least sporadically since the deployment of broadband stations in Vulcano. Previous unrests of Vulcano suggested to be driven by hydrothermal activity did not feature VLP events. Similarly, a causative dike intrusion is not compatible with the long time-series shown in Fig. 5. As discussed above, dike intrusions generate much shorter transient signals even when resulting in large eruptions.

4. Conclusions

The 2021 unrest of Vulcano offers the opportunity to investigate the interplay between fluid flow processes occurring at depth and their effects on the shallow hydrothermal system. Based on available geodetic information, we rule out that a dike may have intruded at shallow depth and instead suggest that deep-seated perturbations may have set in motion magmatic brines rising through the plumbing system of Vulcano. More specifically, we propose that the 2021 and 2018 volcanic unrest at Vulcano are driven by the transient and spasmodic release of brines rising up to the base of the hydrothermal system causing VLPs sequences. Once the fluids enter hydrostatic conditions, they accelerate, H_2O-CO_2 phase separate, H_2O and CO_2 expand, pressuring the hydrothermal system causing microseismicity and extensional deformation. Recognizing this new mechanism has important implications not only for the risk assessment of the region but also for the fundamental understanding of how volcanic systems operate. Our study shows the intimate interplay between tectonics, magmatic activity, and fluid transport processes in active volcanic systems.

CRediT authorship contribution statement

Matteo Lupi: Writing – original draft, Validation, Supervision, Resources, Project administration, Investigation, Formal analysis, Conceptualization. **Salvatore Alparone:** Writing – review & editing, Resources, Project administration, Formal analysis, Data curation, Conceptualization. **Mimmo Palano:** Writing – original draft, Visualization, Methodology, Conceptualization. **Andrea Ursino:** Resources, Formal analysis. **Tullio Ricci:** Project administration, Formal analysis, Conceptualization. **Anthony Finizola:** Methodology, Conceptualization. **Douglas Stumpp:** Methodology. **Iván Cabrera-Pérez:** Software, Methodology. **Geneviève Savard:** Methodology.

Declaration of competing interest

The authors have declare that they have no conflict of interest and that all the data published in the manuscript comply with the ethics of science.

Acknowledgements

The authors wish to thank Gruppo Analisi Dati Sismici of Istituto Nazionale di Geofisica e Vulcanologia—Osservatorio Etneo—Sezione di Catania for providing the earthquakes catalogue. We are also indebted to the technicians of INGV-OE for enabling the acquisition of seismic and geodetic data. Matteo Lupi and Douglas Stumpp are supported for the investigation of high enthalpy geothermal systems by the SNSF project MIGRATE - A Multidisciplinary and InteGRated Approach for geoThermal Exploration (grant number 209434). Tullio Ricci has benefited from funding provided by the "Accordo Quadro tra il Dipartimento della Protezione Civile e l'Istituto Nazionale di Geofisica e Vulcanologia 2022-2025". The contents of this article represent the authors' ideas and do not necessarily correspond to the official opinion and policies of the Dipartimento della Protezione Civile - Presidenza del Consiglio dei Ministri.

Appendix A. Supplementary data

Supplementary material related to this article can be found online at https://doi.org/10.1016/j.jvolgeores.2025.108410.

Data availability

The data that has been used is confidential.

References

Ágústsdóttir, T., Woods, J., Greenfield, T., Green, R.G., White, R.S., Winder, T., Brandsdóttir, B., Steinthórsson, S., Soosalu, H., 2016. Strike-slip faulting during the 2014 Bárðarbunga-Holuhraun dike intrusion, central iceland. Geophys. Res. Lett. 43 (4), 1495–1503.

Aiuppa, A., Bitetto, M., Calabrese, S., Delle Donne, D., Lages, J., La Monica, F.P., Chiodini, G., Tamburello, G., Cotterill, A., Fulignati, P., et al., 2022. Mafic magma feeds degassing unrest at Vulcano Island, Italy. Commun. Earth Environ. 3 (1), 255.

Alparone, S., Bonforte, A., Gambino, S., Guglielmino, F., Obrizzo, F., Velardita, R., 2019. Dynamics of Vulcano Island (Tyrrhenian Sea, Italy) investigated by long-term (40 years) geophysical data. Earth-Sci. Rev. 190, 521–535.

Alparone, S., Cannata, A., Gambino, S., Gresta, S., Milluzzo, V., Montalto, P., 2010. Time-space variation of volcano-seismic events at La Fossa (Vulcano, Aeolian Islands, Italy): new insights into seismic sources in a hydrothermal system. Bull. Volcanol. 72 (7), 803–816.

Barberi, G., Di Grazia, G., Ferrari, F., Firetto Carlino, M., Giampiccolo, E., Maiolino, V., Mostaccio, A., Musumeci, C., Scaltrito, A., Sciotto, G., Tuvè, T., & Ursino, A., 2020. Aeolian islands revised seismic catalog from 2020 (AeolianRSC2020). Istituto Nazionale di Geofisica e Vulcanologia (INGV), URL http://eqcatalog.ct.ingv.it/AeolianRSC/main.asp.

Blanco-Montenegro, I., De Ritis, R., Chiappini, M., 2007. Imaging and modelling the subsurface structure of volcanic calderas with high-resolution aeromagnetic data at Vulcano (Aeolian Islands, Italy). Bull. Volcanol. 69 (6), 643–659.

Carapezza, M., Barberi, F., Ranaldi, M., Ricci, T., Tarchini, L., Barrancos, J., Fischer, C., Perez, N., Weber, K., Di Piazza, A., et al., 2011. Diffuse CO2 soil degassing and CO2 and H2S concentrations in air and related hazards at Vulcano Island (Aeolian arc, Italy). J. Volcanol. Geotherm. Res. 207 (3–4), 130–144.

Cesca, S., Sugan, M., Rudzinski, Ł., Vajedian, S., Niemz, P., Plank, S., Petersen, G., Deng, Z., Rivalta, E., Vuan, A., et al., 2022. Massive earthquake swarm driven by magmatic intrusion at the Bransfield Strait, Antarctica. Commun. Earth Environ. 3 (1), 89.

Chiarabba, C., Pino, N., Ventura, G., Vilardo, G., 2004. Structural features of the shallow plumbing system of Vulcano Island Italy. Bull. Volcanol. 66 (6), 477–484.

Chiodini, G., Frondini, F., Raco, B., 1996. Diffuse emission of CO2 from the Fossa crater, Vulcano Island (Italy). Bull. Volcanol. 58 (1), 41–50.
Christenson, B., Reyes, A., Young, R., Moebis, A., Sherburn, S., Cole-Baker, J., Britten, K., 2010. Cyclic processes and factors leading to phreatic eruption events: Insights from the 25 September 2007 eruption through Ruapehu Crater Lake, New Zealand. J. Volcanol. Geotherm. Res. 191 (1–2), 15–32.
Cintorrino, A.A., Palano, M., Viccaro, M., 2019. Magmatic and tectonic sources at Vulcano (Aeolian Islands, Southern Italy): A geodetic model based on two decades of GPS observations. J. Volcanol. Geotherm. Res. 388, 106689.
Cox, S., 2010. The application of failure mode diagrams for exploring the roles of fluid pressure and stress states in controlling styles of fracture-controlled permeability enhancement in faults and shear zones. Geofluids 10 (1–2), 217–233.
De Astis, G., Lucchi, F., Dellino, P., La Volpe, L., Tranne, C., Frezzotti, M., Peccerillo, A., 2013. Geology, volcanic history and petrology of Vulcano (central Aeolian archipelago). Geol. Soc. Lond. Memoirs 37 (1), 281–349.
Di Giuseppe, M.G., Isaia, R., Troiano, A., 2023. Three-dimensional magnetotelluric modeling of Vulcano Island (Eolie, Italy) and its implications for understanding recent volcanic unrest. Sci. Rep. 13 (1), 16458.
Di Martino, R., Gurrieri, S., Camarda, M., Capasso, G., Prano, V., 2022. Hazardous changes in soil CO2 emissions at Vulcano, Italy, in 2021. J. Geophys. Res.: Solid Earth 127 (11), e2022JB024516.
Di Traglia, F., Bruno, V., Casu, F., Cocina, O., De Luca, C., Giudicepietro, F., Macedonio, G., Mattia, M., Monterroso, F., Privitera, E., et al., 2023. Multi-temporal InSAR, GNSS and seismic measurements reveal the origin of the 2021 vulcano island (Italy) unrest. Geophys. Res. Lett. 50 (24), e2023GL104952.
Dzurisin, D., 2006. Volcano Deformation: New Geodetic Monitoring Techniques. Springer Science & Business Media.
Efron, B., 1982. The Jackknife, the Bootstrap and Other Resampling Plans. Monograph 38, SIAM, Philadelphia.
Federico, C., Cocina, O., Gambino, S., Paonita, A., Branca, S., Coltelli, M., Italiano, F., Bruno, V., Caltabiano, T., Camarda, M., et al., 2023. Inferences on the 2021 ongoing volcanic unrest at vulcano island (Italy) through a comprehensive multidisciplinary surveillance network. Remote. Sens. 15 (5), 1405.
Fournier, R.O., 1999. Hydrothermal processes related to movement of fluid from plastic into brittle rock in the magmatic-epithermal environment. Econ. Geol. 94 (8), 1193–1211.
Gaudin, D., Ricci, T., Finizola, A., Delcher, E., Alparone, S., Barde-Cabusson, S., Brothelande, E., Di Gangi, F., Gambino, S., Inguaggiato, S., et al., 2017. Heat flux-based strategies for the thermal monitoring of sub-fumarolic areas: Examples from Vulcano and La Soufrière de Guadeloupe. J. Volcanol. Geotherm. Res. 343, 122–134.
Graham, C., 2011. Numerical simulations of seismicity-induced fluid flow in the Tjörnes Fracture Zone, Iceland. J. Geophys. Res.: Solid Earth 116 (B7).
Harris, A., Maciejewski, A., 2000. Thermal surveys of the Vulcano Fossa fumarole field 1994–1999: evidence for fumarole migration and sealing. J. Volcanol. Geotherm. Res. 102 (1–2), 119–147.
Herring, T., King, R., McClusky, S., et al., 2010. Introduction to Gamit/globk. Massachusetts Institute of Technology, Cambridge, Massachusetts.
Iervolino, I., Cito, P., De Falco, M., Festa, G., Herrmann, M., Lomax, A., Marzocchi, W., Santo, A., Strumia, C., Massaro, L., et al., 2024. Seismic risk mitigation at Campi Flegrei in volcanic unrest. Nat. Commun. 15 (1), 1–14.
Illsley-Kemp, F., Barker, S.J., Wilson, C.J., Chamberlain, C.J., Hreinsdóttir, S., Ellis, S., Hamling, I.J., Savage, M.K., Mestel, E.R., Wadsworth, F.B., 2021. Volcanic unrest at Taupō volcano in 2019: Causes, mechanisms and implications. Geochem. Geophys. Geosystems 22 (6), e2021GC009803.
Inguaggiato, S., Vita, F., Diliberto, I.S., Inguaggiato, C., Mazot, A., Cangemi, M., Corrao, M., 2022. The volcanic activity changes occurred in the 2021–2022 at Vulcano island (Italy), inferred by the abrupt variations of soil CO2 output. Sci. Rep. 12 (1), 21166.
Miller, S.A., Nur, A., 2000. Permeability as a toggle switch in fluid-controlled crustal processes. Earth Planet. Sci. Lett. 183 (1–2), 133–146.
Mogi, K., 1958. Relations between the eruptions of various volcanoes and the deformation of the ground surfaces around them. Bull. Earthq. Res. Inst. 36.
Nicotra, E., Giuffrida, M., Viccaro, M., Donato, P., D'Oriano, C., Paonita, A., De Rosa, R., 2018. Timescales of pre-eruptive magmatic processes at Vulcano (Aeolian Islands, Italy) during the last 1000 years. Lithos 316, 347–365.
Palano, M., Schiavone, D., Loddo, M., Neri, M., Presti, D., Quarto, R., Totaro, C., Neri, G., 2015. Active upper crust deformation pattern along the southern edge of the Tyrrhenian subduction zone (NE Sicily): Insights from a multidisciplinary approach. Tectonophysics 657, 205–218.
Phillipson, G., Sobradelo, R., Gottsmann, J., 2013. Global volcanic unrest in the 21st century: An analysis of the first decade. J. Volcanol. Geotherm. Res. 264, 183–196.
Piochi, M., De Astis, G., Petrelli, M., Ventura, G., Sulpizio, R., Zanetti, A., 2009. Constraining the recent plumbing system of Vulcano (Aeolian Arc, Italy) by textural, petrological, and fractal analysis: the 1739 AD Pietre Cotte lava flow. Geochem. Geophys. Geosystems 10 (1).
Pritchard, M., Mather, T., McNutt, S.R., Delgado, F., Reath, K., 2019. Thoughts on the criteria to determine the origin of volcanic unrest as magmatic or non-magmatic. Phil. Trans. R. Soc. A 377 (2139), 20180008.
Ricci, T., Finizola, A., Barde-Cabusson, S., Delcher, E., Alparone, S., Gambino, S., Milluzzo, V., 2015. Hydrothermal fluid flow disruptions evidenced by subsurface changes in heat transfer modality: the La Fossa cone of Vulcano (Italy) case study. Geology 43 (11), 959–962.
Richter, C., 1958. New dimensions in seismology: Earthquakes are characterized by geographical position, instant of occurrence, depth, and magnitude. Science 128 (3317), 175–182.
Ruch, J., Vezzoli, L., De Rosa, R., Di Lorenzo, R., Acocella, V., 2016. Magmatic control along a strike-slip volcanic arc: The central Aeolian arc (Italy). Tectonics 35 (2), 407–424.
Selva, J., Bonadonna, C., Branca, S., De Astis, G., Gambino, S., Paonita, A., Pistolesi, M., Ricci, T., Sulpizio, R., Tibaldi, A., et al., 2020. Multiple hazards and paths to eruptions: A review of the volcanic system of Vulcano (Aeolian Islands, Italy). Earth-Sci. Rev. 207, 103186.
Sibson, R.H., 1990. Conditions for fault-valve behaviour. Geol. Soc. Lond. Spec. Publ. 54 (1), 15–28.
Sommaruga, C., 1984. Le ricerche geotermiche svolte a Vulcano negli anni'50. Rend. Della Società Ital. Miner. E Pet. 39 (2), 355–366.
Stissi, S.C., Currenti, G., Cannavò, F., Napoli, R., 2023. Evidence of poro-elastic inflation at the onset of the 2021 Vulcano Island (Italy) unrest. Front. Earth Sci. 11, 1179095.
Stumpp, D., Cabrera-Pérez, I., Savard, G., Ricci, T., Aparone, S., Ursino, A., Palano, M., Sparacino, F., Muñoz Burbanom, F., Barat, C., Ruch, J., Bonadonna, C., Reyes Hardy, M., Lupi, M., 2024. Imaging volcanoes during unrest: Ambient noise tomography of a transient plumbing system, Vulcano, Italy. Nat. Geosci. (in preparation).
Tiampo, K., Rundle, J., Fernandez, J., Langbein, J., 2000. Spherical and ellipsoidal volcanic sources at Long Valley caldera, California, using a genetic algorithm inversion technique. J. Volcanol. Geotherm. Res. 102 (3–4), 189–206.
Tibaldi, A., 2015. Structure of volcano plumbing systems: A review of multi-parametric effects. J. Volcanol. Geotherm. Res. 298, 85–135.
Totaro, C., Aloisi, M., Ferlito, C., Orecchio, B., Presti, D., Scolaro, S., 2022. New insights on the active degassing system of the Lipari–Vulcano complex (South Italy) inferred from Local Earthquake Tomography. Sci. Rep. (ISSN: 2045-2322) 12 (1), 1–10. http://dx.doi.org/10.1038/s41598-022-21921-x, URL https://www.nature.com/articles/s41598-022-21921-x.
Ventura, G., 2013. Kinematics of the Aeolian volcanism (Southern Tyrrhenian Sea) from geophysical and geological data. Geol. Soc. Lond. Memoirs 37 (1), 3–11.
Woods, J., Winder, T., White, R.S., Brandsdóttir, B., 2019. Evolution of a lateral dike intrusion revealed by relatively-relocated dike-induced earthquakes: The 2014–15 Bárðarbunga–Holuhraun rifting event, Iceland. Earth Planet. Sci. Lett. 506, 53–63.